Thermoelectric properties of CZTS thin films: effect of Cu-Zn disorder

E. Isotta[1,*], U. Syafiq[1,2,*], N. Ataollahi[1], A. Chiappini[3], C. Malerba[4], S. Luong[5], V. Trifiletti[5], O. Fenwick[5], N.M. Pugno[1,5,6], and P. Scardi[1,*]

[1]Department of Civil, Environmental and Mechanical Engineering, University of Trento, Trento, Italy
[2]Solar Energy Research Institute, National University of Malaysia (SERI-UKM), 43600 Bangi, Selangor, Malaysia
[3]IFN-CNR CSMFO Lab. and FBK Photonics Unit, Trento, Italy.
[4]Italian National Agency for New Technologies, Energy and Sustainable Economic Development (ENEA), Rome, Italy
[5]School of Engineering and Materials Science, Queen Mary University of London, London, United Kingdom
[6]Laboratory of Bio-inspired, Bionic, Nano, Meta Materials & Mechanics, Department of Civil, Environmental and Mechanical Engineering, University of Trento, Trento, Italy

Abstract

Cu-Zn disorder is known to deeply affect kesterite (Cu_2ZnSnS_4, CZTS) due to the low temperature order-disorder phase transition, leading to a random occupation of the two cations in the shared crystallographic planes. This defect complex has been extensively studied in the thin film photovoltaic sector, with considerable efforts in developing methods to quantify disorder. In this study, a preliminary investigation of thermoelectric properties in temperature for thin film CZTS is presented. It is found that Cu-Zn disorder enhances both electrical conductivity and Seebeck coefficient. This can positively affect the thermoelectric performance, showing a mechanism of potential interest for a broad class of quaternary chalcogenides. The order-disorder transition is clearly visible in the electronic properties. This feature is repeatable, with samples from different preparations and groups showing consistent results, qualitatively suggesting electronic measurements as possible methods to quantify disorder. Furthermore, the reversibility of the transition allows the electronic properties to be tuned via specific thermal treatments, pointing to interesting applications in tunable electronics.

Keywords: Kesterite CZTS, order-disorder transition, thin film thermoelectric, Seebeck coefficient, tuneable electronics, Cu-Zn disorder

*Authors to whom correspondence and material request should be addressed: P.S. (paolo.scardi@unitn.it), E.I. (eleonora.isotta@unitn.it), U.S. (muhammad.mustaffa@unitn.it)

1. Introduction

Kesterite (reference formula Cu_2ZnSnS_4, CZTS) has attracted the attention of the photovoltaic community as a promising alternative to $Cu(In,Ga)Se_2$ (CIGS) absorber layers in thin film solar cell technology[1]. It is valued for its good light-harvesting properties, combined with ease of synthesis and fabrication, along with the use of inexpensive, non-toxic, and abundant materials. The highest achieved efficiency in CZTS thin-film solar cells to date is 12.6%[2], despite the Shockley-Queisser limit indicating a theoretical efficiency of up to 32.4%[3]. Reasons for this sluggish development can be, to a certain extent, traced back to the material itself; CZTS possesses a narrow quaternary phase stability range and a certain degree of crystallographic complexity leading to the co-existence of competitive secondary phases and defect complexes. Compositional variations, structural inhomogeneity, high intrinsic defect density and local band-gap and potential fluctuations are particularly pronounced with non-stoichiometric CZTS compositions, such as the Zn-rich/Cu-poor one, which has demonstrated the highest photovoltaic efficiency[4]. However, the device performance is strongly limited by a high carrier recombination rate connected to non-ideal recombination paths induced by the off-stoichiometry, which can often lead to repeatability issues[5].

Among the defects present in CZTS, Cu-Zn antisites have been recently studied in detail due to the discovery of the order-disorder phase transition, which is second order and reversible. Over the critical temperature of 533 K, the Cu^+ and Zn^{2+} cations which share the same crystallographic plane, randomize their positions[6,7]. Thermal history influences the amount of Cu-Zn disorder, but perfect order is thermodynamically impossible to obtain above 0K. For this reason, regardless of the material composition, a certain number of Cu_{Zn}-Zn_{Cu} antisites form at ambient temperature. Despite the role of these antisites on the photovoltaic performance still being the object of debate[8–13], it has been recently suggested that tail-related detrimental defects are associated with growth conditions providing a slow ordering rate and thus highly disordered samples[13].

In recent years, CZTS in bulk form has been investigated for high temperature thermoelectric (TE) applications[14–20]. Little has been explored regarding thermoelectricity in CZTS thin films, despite the vast knowledge acquired in the past two decades on their fabrication[21–23]. TE energy conversion exploits the Seebeck effect, the development of a voltage gradient in a material as a consequence of an applied temperature difference[24]. The TE figure of merit, zT = $\alpha^2 T/\rho\kappa$, is used to assess the performance, where α is the Seebeck coefficient, ρ the electrical resistivity, T the absolute temperature, and κ thermal conductivity. It was recently shown in bulk CZTS that Cu-Zn disorder can be beneficial for the TE performance by boosting the Seebeck coefficient without penalizing electrical conductivity. This was achieved through a modification in the band structure, leading to flatter and more converged bands. This was correlated with the higher crystallographic symmetry of the disordered tetragonal phase with respect to the ordered[17,18].

Therefore, two key-points can be underlined: i) the Cu-Zn disorder can be indicative of poor quality of the as-grown absorber in photovoltaic devices, thus making it essential to be identified, quantified and understood and ii) this same disorder might instead be exploited in other applications such as thermoelectricity[17,18,25] and tunable electronics[26–28], pointing to attractive directions for micro power generation[29,30] and sensing[31], as well as micro-electro-mechanical systems (MEMS)[32].

In this work, we illustrate a simple and inexpensive fabrication of CZTS thin films based on hot injection, which enables good control over film thickness, composition and secondary phases. We present a preliminary investigation of the TE properties of CZTS thin films synthetized with different routes and show a method to improve the TE performance. Moreover, this work shows the film's strong dependence of the electronic properties on cooling history, connected with the Cu-Zn disorder. This feature is revealed to be advantageous both as a possible diagnostic method for sample quality in solar-cell research, and as an opportunity for applications in tunable electronics.

2. Experimental Section

2.1. Synthesis of CZTS nanoparticle ink

Copper (II) chloride dihydrate ($CuCl_2 \cdot 2H_2O$, >99.0%), zinc chloride ($ZnCl_2$, >98.0%), and tin (II) chloride ($SnCl_2$, 98%) were purchased from Sigma-Aldrich Inc. and dehydrated in vacuum at 200 °C. Sulfur (S), oleylamine (OLA, 70%), toluene (99.9%), and ethanol (>99%) were also purchased from Sigma-Aldrich Inc. and used without further purification.

A CZTS nanoparticle ink was prepared according to the method described by Syafiq et al.[33], with a modified setup for N_2 and vacuum lines as shown in Figure S1 (Supplementary Material, Supplementary Note SN 1). Precursor solutions were prepared by mixing 0.538 g of $CuCl_2 \cdot 2H_2O$, 0.414 g of $ZnCl_2$ and 0.410 g of $SnCl_2$ into a 250 ml three-necked round-bottomed flask containing 6.6 ml of oleylamine (OLA). OLA was added to work both as a solvent and as a capping agent for the CZTS nanoparticles. The solution was stirred and heated in a silicon (Si) oil bath. The mixture was heated to 130°C, then degassed and refilled with N_2 several times before being kept under vacuum. Next, 10 ml of S/OLA 1 M solution (prepared by dissolving 0.449 g S in 10 ml OLA) was rapidly injected in the solution upon reaching ~270°C. The mixture was kept at 270°C for 30 min after the injection and then cooled naturally to room temperature. The obtained suspension of nanoparticles was washed with a mixture of 5 mL toluene and 25 mL ethanol and centrifuged for 10 min at 12000 rpm to separate the solvent from the nanoparticles. Finally, the CZTS nanoparticles were extracted by removing the supernatant, dispersed in toluene, and sonicated to obtain an ink with the desired concentration.

2.2. CZTS thin film deposition and thermal treatment

The deposition was done on soda-lime glass (SLG) substrates. SLG substrates were manually cleaned with soap, treated with concentrated potassium hydroxide (KOH) in ethanol, rinsed with distilled water and ethanol, and finally dried using compressed air. 1 g/ml CZTS nanoparticle ink was used for the deposition of CZTS thin films with different thicknesses. For a thinner film, deposition was done by a spin-coating method (50 μl ink at 2000 rpm for 30 s). Deposition of thicker films was done by the doctor blade technique.

Two stages of thermal treatment were performed on the deposited CZTS thin films[34]. The thermal treatment was done inside a quartz tube furnace connected to separate vacuum, N_2, and exhaust lines. For the first stage, the tube was pumped down to ~3.0×10^{-1} mbar. The tube was then flushed with N_2 to purge the system of residual air, and the temperature ramped up to 500°C at 3°C/min and kept stable for 1 hour. The annealed sample was then cooled down to room temperature in a continuous flow of N_2. CZTS thin films were then taken out to be annealed in the presence of an excess amount of S for the second stage of thermal treatment. The procedure for the second thermal treatment follows the first, except for the annealing temperature which was set at 560°C[35].

2.3. CZTS Thin Film Characterization

The morphology of CZTS thin film samples was observed by scanning electron microscopy (SEM), using a JEOL JSM-7001F FEG-SEM (JEOL, Tokyo, Japan) equipped with an energy-dispersive x-ray spectroscopy detector (EDXS, Oxford INCA PentaFETx3, Oxford, United Kingdom). Observations were made at 10.00-15.00 keV electron beam energy with a working distance of 5-10 mm. Surface morphology images were acquired in a top-down configuration, whereas a cross-sectional analysis was performed by putting the cross-section of the film on a 90° stub.

X-ray diffraction (XRD) patterns were collected in Bragg-Brentano geometry with a Cu-K_α radiation source (Rigaku PMG, Tokyo, Japan) for 1.5 μm and 30 μm-thick samples, obtained respectively by spin-coating and by doctor-blade deposition from the same ink. A Rietveld-refinement of XRD data was performed with the TOPAS 7 software package, with the aid of Whole Powder Pattern Modelling (WPPM) macros for size analysis.[36,37]

Raman spectra were collected using a LabRAM Aramis (Horiba Jobin-Yvon) equipped with an optical microscope and a 100X objective. Diode-pumped solid-state laser sources of 532 nm and 785 nm were used for the excitation of the Raman signal that was detected with an air-cooled charge-coupled device. The overall acquisition time was 10 s with laser powers of 1.8 mW (532 nm) and 2.3 mW (785 nm). A fit of the Raman spectra was performed with the software PM2K[38]. Although specifically designed for the analysis of XRD patterns, the software is easily adapted to the analysis of Raman spectra, using a set of nine Lorentzian

peaks. The background was removed to allow comparison with previous works[6]. Spectra with background are shown in Figure S2 (Supplementary Material, SN 2).

Electrical resistivity and Seebeck coefficient measurements were performed with a Linseis LSR-3 Meter in the temperature range 320–720 K. Resistivity was measured in 2-contact configuration with the aid of a thin film adapter for high resistance samples. The Seebeck coefficient was measured in 4-contact configuration with Pt standard and a temperature gradient of 10K.

In-plane thermal conductivity measurements were performed with a Linseis Thin Film Analyser. The measurement is done on a suspended Si_3N_4 membrane incorporated on a pre-patterned measurement chip using a quasi-steady state 3-ω method. The measurement, which is performed under vacuum and in the dark, is described in detail elsewhere.[39–41]

3. Results and Discussion

3.1. Morphological and structural characterization

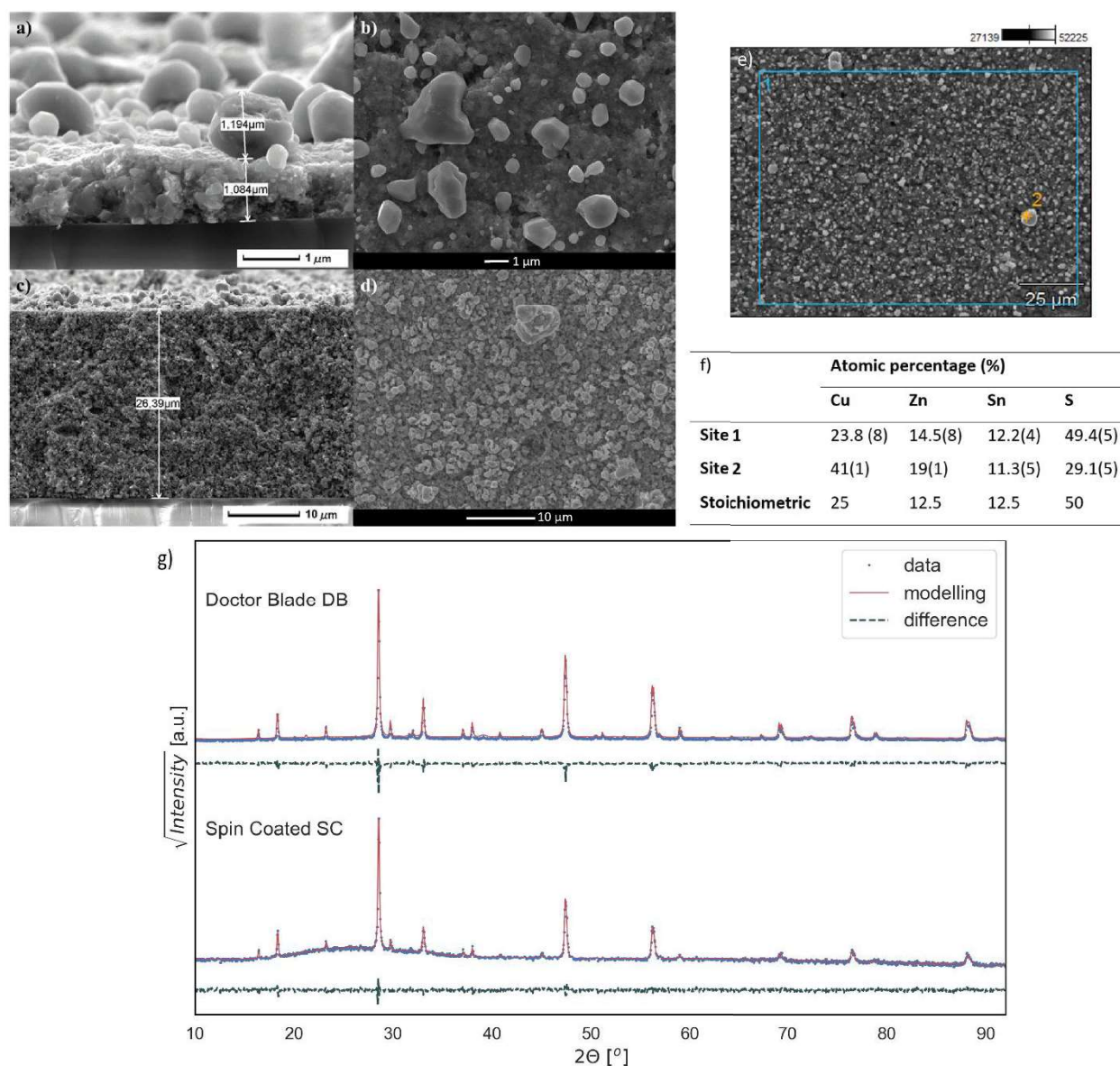| f)	Atomic percentage (%)			
	Cu	Zn	Sn	S
Site 1	23.8 (8)	14.5(8)	12.2(4)	49.4(5)
Site 2	41(1)	19(1)	11.3(5)	29.1(5)
Stoichiometric	25	12.5	12.5	50

Figure 1. Cross-section and surface SEM images of CZTS thin film deposited by spin-coating (a,b) and via the doctor blade method (c,d). Surface of the CZTS thin film (spin coating) used for EDXS analysis (e). The table in panel f) shows the atomic percentage of each element in CZTS from EDXS. g) XRD data refinement for a spin coated and a doctor blade films. The two patterns have been simultaneously refined with a unique kesterite model (see text for details).

SEM micrographs show that the thin films made by spin-coating (SC samples from here on, Figure 1a-b) consist of a □1.0 µm thick uniform layer of CZTS nanoparticles with some micrograins (>1.0 µm in size) scattered on top. The films deposited via the doctor blade method (DB samples from here on, Figure 1c-d) were much thicker (□26 µm), but had a similar surface morphology.

The elemental composition from EDXS analysis (Figure 1e-f, referring to the SC sample) shows a Zn-rich Cu-poor composition for the whole film (site 1), classified as A-type CZTS according to the notation introduced by Lafond et Al.[42] The S content is close to stoichiometric, a feature that is believed to promote a faster Cu-Zn ordering (or disordering) through a higher density of cation vacancies, according to a recent study by Larsen et Al [13]. Large and isolated particles (>5 µm in size) on top of the SC film (site 2) show a Cu-rich stoichiometry that could originate from a partial segregation of Cu from the film.

XRD patterns, data modelling and corresponding residuals for the SC and DB samples are plotted in Figure 1g. The two sets of XRD data have been refined simultaneously, modelled with the same tetragonal $I\text{-}42m$ kesterite phases. The samples present a good phase purity, with a minor fraction (3(1)% of total weight) of chalcocite Cu_2S, that we speculate connected with the superficial Cu-rich particles seen in SEM. A macro to correct for the absorption of thin films[43] has been used for the SC sample, that, based on the decay of intensity at larger angles, estimates a sample thickness of ~1.8 µm (assuming a theoretical density of 4.56 g/cm³), in good agreement with the SEM micrographs. For this film, two broad peaks have been added to model the contribution of the SLG substrate, visible in the lower angle region of the pattern. This was not necessary for the DB film, as the radiation is entirely absorbed within the thicker kesterite layer. The modelling of the kesterite peak profiles requires two CZTS phases, a coarser one (with mean crystal-domain size estimated in the range of 0,5(2) µm) and a finer one (around 10(8) nm), to account for the large dispersion of crystal-domain dimensions in the samples, a feature suggested by the SEM micrographs (Figure 2). A similar bimodal distribution was observed by TEM in a previous study on kesterite powders, although prepared using a different technique.[16,17] Cell parameters display a slight variation between the two phases and are estimated as a = 5.437 Å and c = 10.848 Å for the coarser phase, and a = 5.416 Å and c = 10.896 Å for the finer phase. For both samples, the coarser kesterite phase appears to be present in the largest fraction (65% and 73% in total weight of kesterite, respectively for the SC and DB sample).

3.2. Raman spectroscopy

For the following discussion, two typologies of spin-coated samples were considered: a "slowly cooled" sample, which is the sample as-is after the thermal treatment described above, and a "quenched" sample, where a post-annealing step at 350°C is added (performed in glovebox loaded with N_2 atmosphere, heating rate of 3 K/min) followed by a fast quenching to room temperature. This has been done to promote the disordered kesterite phase by retaining the high-temperature Cu-Zn disorder; this is known to develop in ordered tetragonal kesterite above 533K, when the two cations randomly occupy the intermediate planes of the structure (4d Wyckoff sites).[44,45] Ordered and disordered kesterite (respectively with space group $I\text{-}4$ and $I\text{-}42m$, illustrated in Figure 2a-b) due to the identical electronic configurations of the Cu^+ and Zn^{2+} cations, are known to be undistinguishable with XRD[17]. However, a certain difference can be observed with near-resonance Raman spectroscopy, due to the sensitivity of the method to the local atomic environment.[44] This is deemed one of the most reliable methods reported to date to quantify Cu-Zn disorder.

Raman spectra (Figure 2c) for the slowly cooled and quenched samples were collected and all the peaks correspond to kesterite modes, as reported in the literature.[44,46]

In agreement with Scragg et Al.[6,45], for the disordered quenched sample we observe a broadening of the first A mode (labelled m_{1A}). For the 785 nm excitation source, Raman modes appear of modest intensity upon a sloped background associated with photoluminescence effects (see Figure S2, Supplementary Material, SN 2). This lack of signal results in a large scatter in the data (Figure 2c, lower right) that does not allow a reliable identification of peaks and their intensities. Despite this, the observation on the relative

intensities between m_{2A} and modes m_{3A}, m_{4E} and m_{5B} still seems to hold true: for the slowly cooled sample m_{2A} is greater than the others, while for the quenched film this difference is smoothed out.

The same authors[44,45,47] proposed two parameters as indictors of the order state, retrieved from Raman spectra collected with 785 nm excitation source. The first is the full width at half maximum (FWHM) of the first A mode, which is larger for more disordered samples, the second is the parameter Q, defined as Q = $I(m_{2A})/I(m_{3A})$, which is larger for more ordered samples. The same group derived an order parameter S for the Cu-Zn order-disorder transition, defined as S = $2(P^{Cu}_{Cu} -1/2)$, where P^{Cu}_{Cu} is the probability of finding a Cu atom in its proper lattice site. S=1 means perfect order, whereas S=0 stands for full disorder. The relationship they propose between the Raman-derived parameter Q and the order parameter S is linear and is expressed as S = (0.18 +- 0.02)Q.[44,45,47]

For our slowly cooled sample, FWHM (m_{1A}) ~ 6 cm^{-1} and Q ~ 4, both in accordance with literature values for ordered samples.[44] S = 0.72(8) for this sample. For the quenched sample FWHM (m_{1A}) ~ 8 cm^{-1}, whereas a quantification of the intensities of m_{2A} and m_{3A} modes proves extremely difficult. A tentative estimate gives Q ~ 1.18 and S ~ 0.21(2). Despite uncertainties deriving from the fitting of low intensity peaks, values of FWHM, Q and S in this range would indicate a highly disordered sample.

The drop in spectral intensity in this last case could be due to a shift away from resonance conditions[45], as the bandgap gets smaller with respect to the excitation wavelength (785 nm = 1.58 eV). UV-Vis spectroscopy (in Supplementary Material, SN 3, Figure S3) confirms this trend of the bandgap, estimated as
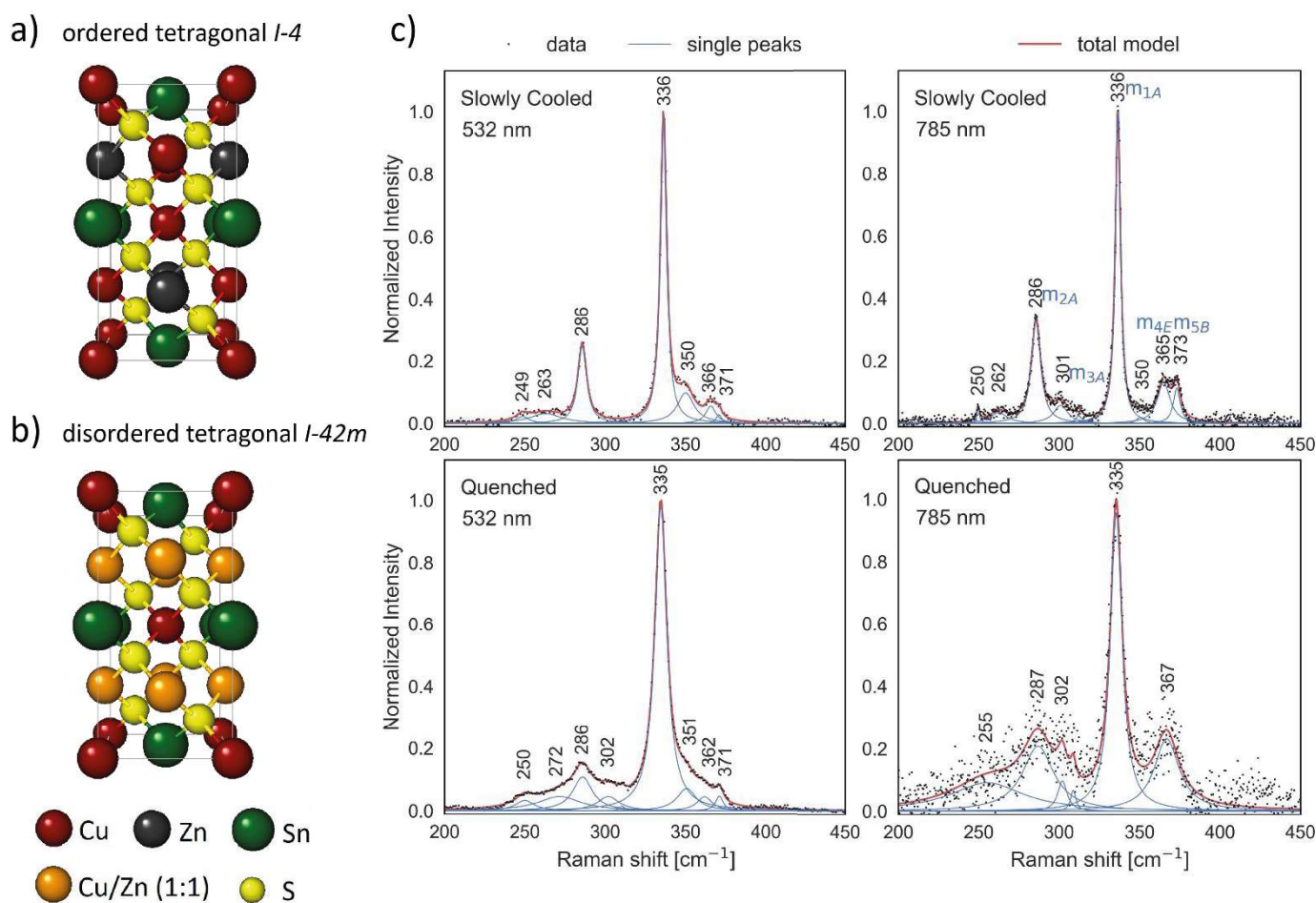

Figure 2. Crystal structures of tetragonal ordered kesterite, s.g. *I-4* (a), and of tetragonal disordered, s.g. *I-42m* (b), involving a randomization of Cu$^+$ and Zn^{2+} cations in the intermediate planes (*2c* and *2d* Wyckoff positions in the ordered becoming a unique *4d* site in disordered). c) Near-resonant Raman spectroscopy and peak fitting using Lorentzian curves. A sample slowly cooled after the thermal treatment and another quenched from a 350°C post-annealing are shown, both measured with excitation wavelengths of 532 nm and 785 nm. Intensities are normalized with respect to the main mode. Mode labelling can be seen in the upper right quadrant.

1.62 eV for the slowly cooled sample and 1.50 eV for the quenched sample. This is in agreement with literature reports of CZTS bandgap variability with disorder.[9]

In any case, this loss of signal makes it difficult to reliably quantify the peak intensities and can limit the applicability of the Raman measurement for the estimation of Cu-Zn disorder. For this reason, we put forward a complementary technique to track disorder, based on clearly distinguishable and quantifiable signals.

3.3. Thermoelectric properties of spin-coated samples

The electronic transport properties (electrical resistivity, ρ, and Seebeck coefficient or thermopower, α, which combined give the Power Factor, PF= α^2/ρ) for a slowly cooled and a quenched spin-coated film are visible in Figure 3a-c. The slowly cooled sample presents high ρ and low α values in the lower-temperature range. Between 450K and 550K the thermopower displays a sharp rise, remaining then high for higher temperatures. The electrical resistivity presents a generally decreasing trend, evidencing the semiconducting nature, only perturbed by a small kink in the range 450K-550K.

We believe these features to be the hallmark of the order-disorder transition. Indeed, as predicted by ab-initio simulations, and experimentally verified in recent work from some of the authors[17,18] the phase transition from ordered *I-4* to disordered *I-42m* tetragonal CZTS leads to a modification in the electronic band structure which strongly affects the electronic properties.

With the disordered structure, the top three valence bands tend to converge significantly and to become flatter. Band convergence (or band degeneracy N_V) is a known mechanism in thermoelectricity that can decouple the trends of α and ρ[48,49]. Moreover, the increased flatness of the bands happening with disorder implies a higher inertial effective mass of charge carriers m_I^*. Both these effects are significant as the Seebeck coefficient is directly proportional to the density of state effective mass $m_{DOS}^* = N_V^{2/3} m_I^*$.

For these reasons, the transition from ordered to disordered CZTS, happening around 533K, leads to a sharp rise in the thermopower.

At the same time, the electrical resistivity trend does not present significant features at the transition. A reason for this could be that on one side band degeneracy can improve the carrier concentration, on the other, the increased m_I^* implies a lower carrier mobility. This double effect (improved carrier concentration and decreased carrier mobility) has been experimentally verified on bulk polycrystalline samples in[18] and leads to a not-much-affected electrical resistivity trend. The calculation of the band structures, carrier mobility and concentration data, as well as more detailed explanations of the mechanisms can be found in[18]. In another article[17], instead, thermal analyses show that the observed sharp rise in Seebeck coefficient is associated with a second-order and reversible transition with critical temperature of 533K (i.e. the order-disorder transition[44]).

The electronic properties of the slowly cooled and quenched spin-coated films (Figure 3a-c) are in accordance with previous theoretical predictions and experimental observations on bulk polycrystalline samples. Indeed, for the slowly cooled sample the progressive development of Cu-Zn disorder leads to the enhancement of the Seebeck coefficient, localized in the proximity of the transition critical temperature of 533K. The effect is particularly evident as the sample starts from an ordered condition (S estimated ~0.7). The electrical resistivity trend is instead not much affected, likely due to reasons explained above. The quenched sample, given its initial disordered state (S estimated ~0.2), exhibits a "disordered behavior" straight from the beginning of the measurement, with lower electrical resistivity and higher Seebeck coefficient values. The trends consistently show reduced transition-specific features around 533 K, as allegedly little of the sample is performing the order-disorder transition.

Results are in good agreement with what has been reported for bulk CZTS TE samples.[17,18,50] It is noticeable that, with respect to these, thin film measurements present a sharper variation of electronic properties at the transition (see for example the Seebeck coefficient curve in [17]), possibly due to different kinetics of the phase transition. This can also originate from a different temperature-homogenization between bulk and thin film samples.
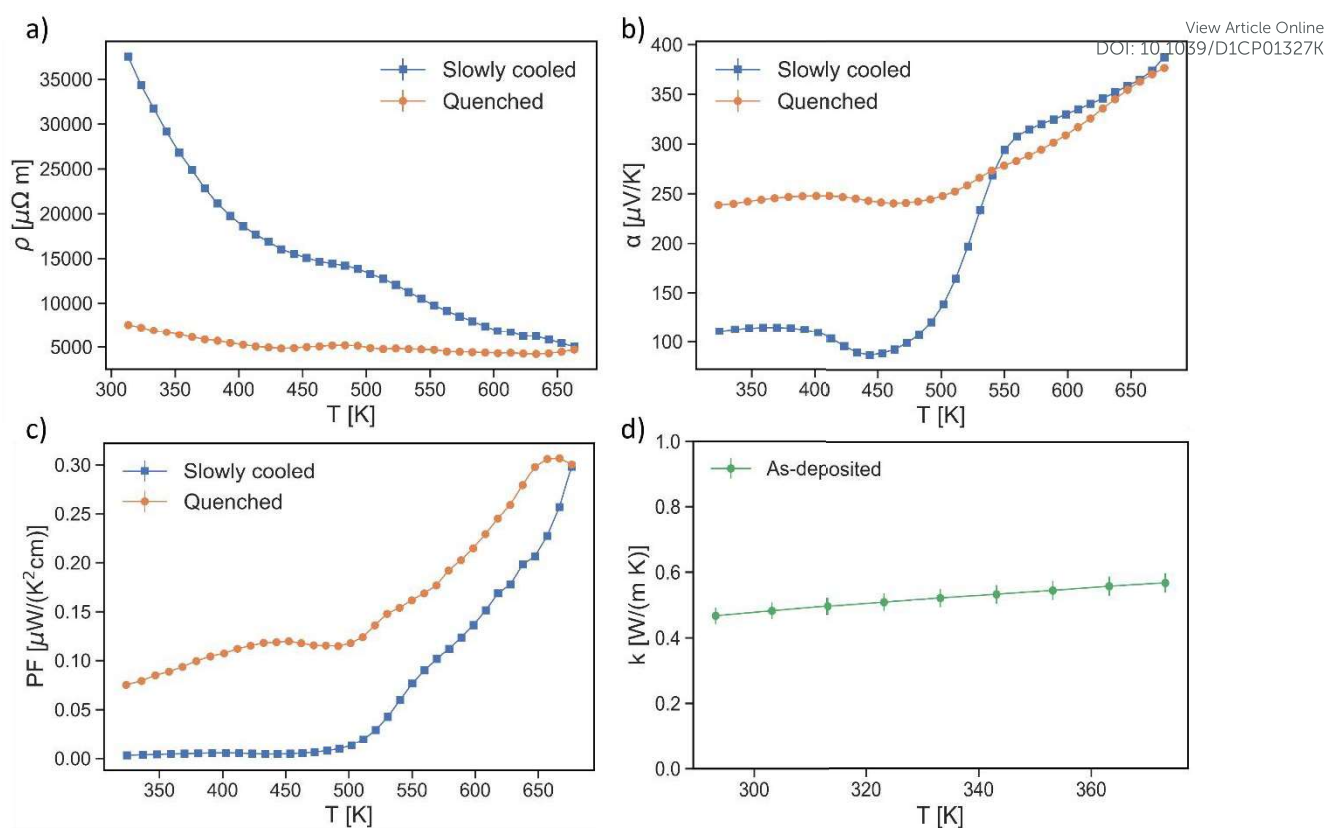
Figure 3. Electrical resistivity ρ (a), absolute Seebeck coefficient α (b) and Power Factor PF (c) for spin-coated CZTS thin films. A sample after slow cooling (blue, squared markers), initially in an ordered state, and a sample after quenching from a 350°C post-annealing (orange, circular markers), in a disordered state, have been measured. d) Thermal conductivity (k) for the as-deposited spin-coated sample.

As expected, the disordered quenched sample presents a higher PF and a weaker dependence on temperature.

Figure 3d shows a measurement of thermal conductivity k for an as-deposited sample. k was measured by the in-plane 3Ω method, depositing the sample on a thin (~100 nm) Si_3N_4 membrane incorporated on a silicon chip with pre-patterned electrodes. This allows in-plane measurements, in line with the other thermoelectric measurements in Figure 3. On the other hand, the delicate nature of the Si_3N_4 membrane prevented the thermal treatment of the sample at 560 °C, as this damaged the measurement chips. We therefore limited our analysis on as-deposited samples (only with annealing at 100 °C, performed in a glove box). The absence of treatment and different surface energy of the Si_3N_4 compared to SLG may induce a different morphology in the film and a different Cu-Zn order parameter, S. SEM images (Figure S4, Supplementary material) on corresponding chip- and SLG-deposited samples do, however, show that both films are continuous and pin-hole free. No major morphological differences are observed. We can also confirm a smaller grain size than in the films on SLG as expected from the lower annealing temperature. From the literature, CZTS is known to possess a comparably low k[20] among TE materials, and indeed the film presents values below 0.6 W/mK. This is associated in general to the crystallographic complexity of CZTS, often subject to cation disorder, and additionally, in this specific case, to the higher density of grain boundaries associated with the lack of thermal treatment.

Geometrical measurements of density yield values >93% (see Supplementary Material, SN 5).

To estimate zT for the thermally treated films we calculated the thermal conductivity from the lattice component (k_L) of a polycrystalline bulk sample, corrected for the electronic component (k_e) of the thin film sample. Results, calculations, and assumptions of the method are presented in detail in the Supplementary Material, SN 6. As expected for the resistive nature of the samples, k_e makes little contribution to the overall k. The calculated thermal conductivity is in the order of 0.65 W/mK, 10-20 % higher than the measured value for the as-deposited sample. An increase is expected upon thermal annealing as the thermal treatment should promote domain growth and improved connection of domains, thus reducing phonon scattering.

An estimate of zT can be obtained from the PF data and the calculated values of k and yield a maximum of ~0.035 at 673K. Despite the considerable level of uncertainty in the calculation (speculated as at least ~30%), this estimation of zT is in accordance with literature values for pristine CZTS bulk samples[14,15,19,20]. The quenched sample presents comparatively higher values of PF, especially in the low temperature range. Given the small contribution of k_e to k, this is expected to positively contribute to the real zT value, suggesting that Cu-Zn disorder can overall lead to a higher TE performance.

3.4. Perspectives and applications of disorder-induced variation of transport properties

These results highlight the role of Cu-Zn disorder in promoting better electronic properties. Moreover, and possibly more importantly, they qualitatively show how electronic properties can mark a difference between samples in diverse order states. This dependence has two important consequences.

First, due to the difficulty of other techniques in reliably determining the level of Cu-Zn disorder, electronic properties could be used as complementary methods for diagnostic purposes. Second, the dependence of Cu-Zn disorder on the thermal history opens the path to the possibility of tuning the electronic properties of CZTS.
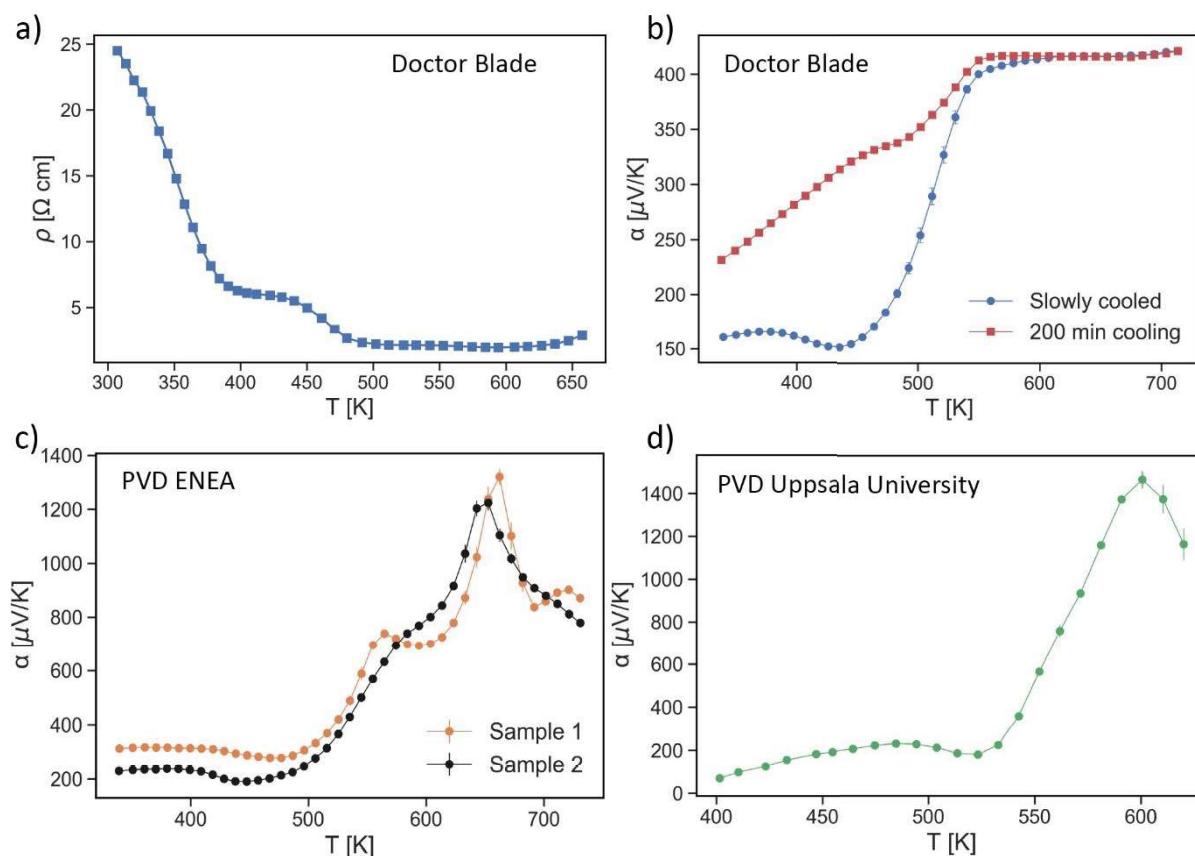

Figure 4: Electrical resistivity (a) and Seebeck coefficient (b) for a doctor-blade deposited sample (University of Trento). Seebeck coefficient for two samples obtained with co-sputtering of SnS, ZnS and Zn (c, ENEA, Rome) and CuS, ZnS and SnS (d, Ångström Laboratory, Uppsala University) with successive sulfurization.

Regarding the first issue, the Seebeck coefficient measurement can efficiently track the progression of the order-disorder transition: as Cu-Zn disorder increases, the symmetry-induced band degeneracy progressively increases the thermopower. This feature is observed in nanocrystalline bulk[17,18,51] and thin film samples from different preparation routes. Figure 4 shows measurements performed on thin film samples grown by sulfurization of precursors deposited via with doctor blade (University of Trento, Figure 4a-b) or physical vapor deposition (PVD) methods: co-sputtering of SnS, ZnS and Cu (ENEA Rome, Figure 4c)[8] and co-sputtering of CuS, SnS and ZnS (Ångström Laboratory, Uppsala University, Figure 4d)[52–55]. The

Seebeck coefficient and electrical resistivity (available only for the doctor blade sample) present a trend comparable to the spin-coated samples. Although always observable, the quantitative jump in Seebeck coefficient seem to depend on the preparation method. The same applies for electrical resistivity values. A reason for this could be a difference in carrier concentration which is tentatively connected to stoichiometry fluctuations or differences in crystallinity and grain size. What is relevant, though, is that the electronic properties show a clear dependence from the level of Cu-Zn disorder. Upon a suitable calibration that considers preparation differences, they could be used as second order parameters to retrieve the starting level of disorder in the sample. In particular, the increase in Seebeck coefficient at the transition seems to be the most sensitive and sample-robust feature. A proposed methodology to do it would be:

(i) prepare a large set of samples characterized by different thermal histories.

(ii) For each sample, associate the TE feature (e.g. a thermopower increase of ~200 µV/K for our slowly cooled and of ~30 µV/K for our quenched samples) with the order parameter (e.g. 0.72(8) slowly cooled and 0.21(2) quenched), possibly verified with more than one technique.

(iii) Derive a functional relationship between the TE feature and the order parameter. One thing to bear in mind is that a linear relationship, although intuitive, might not be totally accurate for electronic properties. (e.g. the Seebeck coefficient if a two-phase medium, as a partially disorder sample could be approximated to, is typically calculated with an average weighted on the electrical conductivity[9])

Preliminary derivations of an order parameter have been performed for bulk CZTS samples[56]. We believe this method could represent an interesting, easy, and accessible diagnostic technique for determining Cu-Zn disorder. Its good sensitivity, given the clear features at the transition, could complement techniques like Raman spectroscopy when losing accuracy for highly disordered samples. Limitations of this method include that a correction factor needs to be applied to account for the differences observed in the diverse preparation routes. Furthermore, it is "distructive", as exposing the sample to high temperatures for the TE measurement would definitely change the initial level of Cu-Zn order. A twin copy of the sample of interest should therefore be utilized.

Regarding the exploitation of Cu-Zn disorder for tunability purposes, as a proof of concept, Figure 5 illustrates how electrical resistivity and Seebeck coefficient vary with varying cooling rates applied to the same sample. Different thermal histories lead to different levels of disorder, and indeed the shorter the cooling rate, the lower and flatter are the resistivity curves (Figure 5a). Similarly, upon fast cooling, the increase in Seebeck coefficient at the transition is smoothed, and less difference is observed in the values before and after the transition region (Figure 5b but also Figure 4b). Figure S8 and comments therein show the repeatability of measurements within the same cycle (Supplementary Material, SN 7). It is relevant to point out that due to the reversible nature of the transition, these paths can be covered interchangeably: the order in which the measurements were performed, for example, is that of the legend, from up to down. Therefore, if the sample is protected from degradation and development of secondary phases (as in the case of these measurements, performed in He atmosphere), one could keep tuning the resistivity curve via varying the disorder level through a suitable thermal history. Furthermore, a large range of values can be achieved, with resistivity potentially covering a full order of magnitude 0.4-4 Ω*cm. This feature might prove relevant and attractive for tunable electronics applications and could open the path to novel functionalities in devices like tunable TE micro-generators and coolers, MEMS, as well as for sensing purposes.
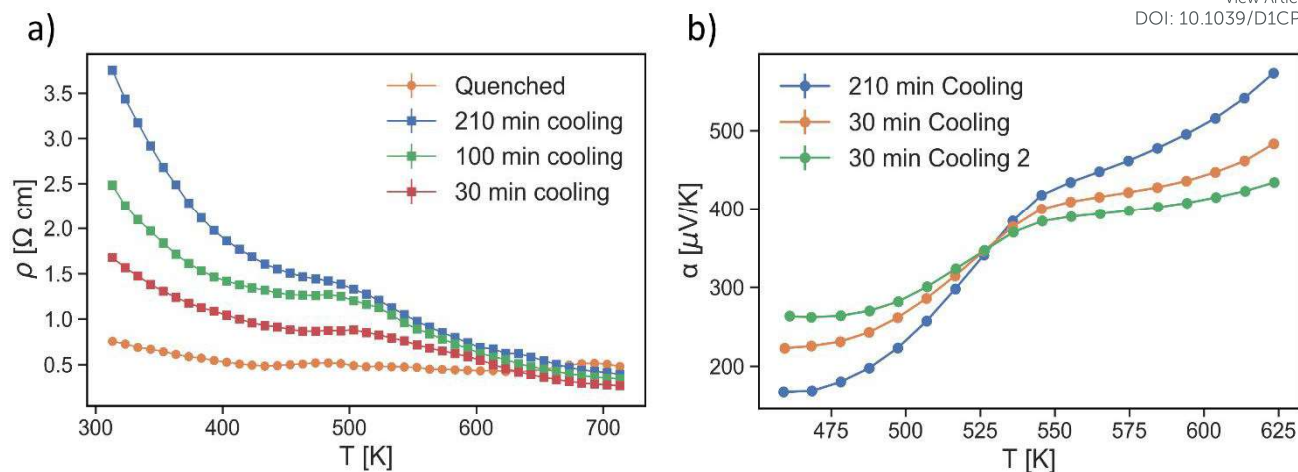
Figure 5: Electrical resistivity (a) and Seebeck coefficient (b) for a spin-coated kesterite thin film sample that has undergone different cooling processes. As visible, the longest the cooling the higher the resistivity values, in association with the achievement of a higher level of ordering. At the same time, short cooling times reduce the increase of the Seebeck coefficient characteristic of the order-disorder transition. This behaviour and the reversibility of the ordering process showcase the possibility of using the material for tunable electronics. The order of measurements is from up to down in the legend.

4. Conclusions

In summary, we have illustrated a facile and cost-effective synthesis method for thin film CZTS based on hot injection and spin coating or doctor blade deposition. SEM, XRD and Raman characterization indicates the formation of good quality kesterite films. A quenching process on some of the samples lead to the development of Cu-Zn disorder, with respect to the more ordered, slowly cooled samples. This disorder is investigated with Raman spectroscopy, which loses sensitivity at high levels of disorder when resonance conditions get weaker. The present study shows that Cu-Zn disorder is not only beneficial for thermoelectricity, but also clearly observable in the trend of electronic properties, unveiling a complementary technique to Raman spectroscopy for the characterization of disorder. This effect is verified on multiple samples from different groups and preparation methods. The derivation of a quantitative relationship between the increase in Seebeck coefficient and/or the value of electrical resistivity and the Cu-Zn order parameter will be the subject of future work, possibly connecting it with the effect of different elemental compositions and preparation methods.

Finally, a proof-of-concept experiment is presented which successfully shows that by tuning the thermal history, electrical resistivity and Seebeck coefficient values can be reversibly modified. This reveals that the reversible nature of Cu-Zn disorder and the visible impact it has on electronic properties make it an interesting feature to exploit for applications in tunable electronics.

Author contributions

E.I. contributed with XRD, Raman, SEM and TE characterization, data interpretation and discussion, main draft preparation. U.S. contributed with sample preparation, SEM and TE characterization, data interpretation and discussion, main draft preparation. N.A. contributed with sample preparation, reviewing of the draft. A.C. contributed with the Raman characterization. C.M. contributed with providing some samples, reviewing of the draft. S.L, V.T., and O.F. contributed with the thermal conductivity measurements, reviewing of the draft. N.M.P. contributed with funding acquisition and reviewing of the draft. P.S. contributed with conceptualization of the work, funding acquisition, structural characterization, data interpretation and discussion, reviewing and editing of the draft, and supervision of the work.

Physical Chemistry Chemical Physics Accepted Manuscript

Conflicts of interest

There are no conflicts of interest to declare.

References

1   U. Syafiq, N. Ataollahi and P. Scardi, Progress in CZTS as hole transport layer in perovskite solar cell, *Sol. Energy*, 2020, **196**, 399–408.

2   W. Wang, M. T. Winkler, O. Gunawan, T. Gokmen, T. K. Todorov, Y. Zhu and D. B. Mitzi, Device characteristics of CZTSSe thin-film solar cells with 12.6% efficiency, *Adv. Energy Mater.*, 2014, **4**, 1–5.

3   W. Ki and H. W. Hillhouse, Earth-Abundant Element Photovoltaics Directly from Soluble Precursors with High Yield Using a Non-Toxic Solvent, *Adv. Energy Mater.*, 2011, **1**, 732–735.

4   H. Katagiri, K. Jimbo, M. Tahara, H. Araki and K. Oishi, The influence of the composition ratio on CZTS-based thin film solar cells Hironori Katagiri, Kazuo Jimbo, Masami Tahara, Hideaki Araki and Koichiro Oishi Nagaoka National College of Technology, 888 Nishikatakai, Nagaoka, Niigata 940-8532, Japan, *Mater. Res. Soc. Symp. Proc. Vol. 1165*, 2009, **1165**, 1165-M04-01.

5   M. Kumar, A. Dubey, N. Adhikari, S. Venkatesan and Q. Qiao, Strategic review of secondary phases, defects and defect-complexes in kesterite CZTS-Se solar cells, *Energy Environ. Sci.*, 2015, **8**, 3134–3159.

6   J. J. S. Scragg, L. Choubrac, A. Lafond, T. Ericson and C. Platzer-Björkman, A low-temperature order-disorder transition in Cu2ZnSnS4 thin films, *Appl. Phys. Lett.*, 2014, **104**, 2–6.

7   J. J. S. Scragg, J. K. Larsen, M. Kumar, C. Persson, J. Sendler, S. Siebentritt and C. Platzer Björkman, Cu-Zn disorder and band gap fluctuations in Cu $_2$ ZnSn(S,Se) $_4$: Theoretical and experimental investigations, *Phys. status solidi*, 2016, **253**, 247–254.

8   C. Malerba, M. Valentini and A. Mittiga, Cation Disorder in Cu2ZnSnS4 Thin Films : Effect on Solar Cell Performances, *Sol. RRL*, 2017, **1**, 1700101.

9   M. Valentini, C. Malerba, F. Menchini, D. Tedeschi, A. Polimeni, M. Capizzi and A. Mittiga, Effect of the order-disorder transition on the optical properties of Cu2ZnSnS4, *Appl. Phys. Lett.*, 2016, **108**, 211909.

10   G. Rey, G. Larramona, S. Bourdais, C. Choné, B. Delatouche, A. Jacob, G. Dennler and S. Siebentritt, On the origin of band-tails in kesterite, *Sol. Energy Mater. Sol. Cells*, 2018, **179**, 142–151.

11   G. Rey, T. P. Weiss, J. Sendler, A. Finger, C. Spindler, F. Werner, M. Melchiorre, M. Hála, M. Guennou and S. Siebentritt, Ordering kesterite improves solar cells : A low temperature post-deposition annealing study, *Sol. Energy Mater. Sol. Cells*, 2016, **151**, 131–138.

12   M. Lang, T. Renz, A. Opolka, C. Zimmermann, C. Krämmer, M. Neuwirth, H. Kalt and M. Hetterich, Impact of the degree of Cu-Zn order in Cu2ZnSn(S,Se)4 solar cell absorbers on defect states and band tails, *Appl. Phys. Lett.*, 2018, **113**, 1–6.

13   J. K. Larsen, J. J. S. Scragg, N. Ross and C. Platzer-Björkman, Band tails and Cu-Zn disorder in Cu $_2$ ZnSnS $_4$ solar cells , *ACS Appl. Energy Mater.*, , DOI:10.1021/acsaem.0c00926.

14   M. L. Liu, F. Q. Huang, L. D. Chen and I. W. Chen, A wide-band-gap p -type thermoelectric material based on quaternary chalcogenides of Cu2ZnSnQ4 (Q=S,Se), *Appl. Phys. Lett.*, 2009, **94**, 3–6.

15   H. Yang, L. A. Jauregui, G. Zhang, Y. P. Chen and Y. Wu, Nontoxic and abundant copper zinc tin sulfide nanocrystals for potential high-temperature thermoelectric energy harvesting, *Nano Lett.*, 2012, **12**, 540–545.

16   E. Isotta, N. M. Pugno and P. Scardi, Nanostructured kesterite (Cu2ZnSnS4) for applications in thermoelectric devices, *Powder Diffr.*, 2019, 1–6.

17   Isotta, Fanciulli, Pugno and Scardi, Effect of the Order-Disorder Transition on the Seebeck Coefficient of Nanostructured Thermoelectric Cu2ZnSnS4, *Nanomaterials*, 2019, **9**, 762.

18   E. Isotta, B. Mukherjee, C. Fanciulli, N. M. Pugno and P. Scardi, Order–Disorder Transition in Kesterite Cu2ZnSnS4: Thermopower Enhancement via Electronic Band Structure Modification, *J. Phys. Chem. C*, 2020, **124**, 7091–7096.

19   Q. Jiang, H. Yan, Y. Lin, Y. Shen, J. Yang and M. J. Reece, Colossal thermoelectric enhancement in Cu2+xZn1−xSnS4solid solution by local disordering of crystal lattice and multi-scale defect engineering, *J. Mater. Chem. A*, 2020, **8**, 10909–10916.

20   E. Isotta, B. Mukherjee, C. Fanciulli, N. Ataollahi, I. Sergueev, S. Stankov, R. Edla, N. M. Pugno and P. Scardi, Origin of a Simultaneous Suppression of Thermal Conductivity and Increase of Electrical Conductivity and Seebeck Coefficient in Disordered Cubic Cu2ZnSnS4, *Phys. Rev. Appl.*, 2020, **10**, 1.

21   K. V. Gunavathy, K. Tamilarasan, C. Rangasami and A. M. S. Arulanantham, Solution processed copper zinc tin sulfide thin films for thermoelectric device applications, *Ceram. Int.*, 2020, **46**, 28342–28354.

22   Y. Zeng, G. Liang, P. Fan, Y. Xie, B. Fan, J. Hu, Z. Zheng, X. Zhang, J. Luo and D. Zhang, The structural, optical and thermoelectric properties of single target sputtered Cu2ZnSn(S,Se)4 thin film, *J. Mater. Sci. Mater. Electron.*, 2017, **28**, 13763–13769.

23   A. Ashfaq, J. Jacob, N. Bano, A. Ali, W. Ahmad, K. Mahmood, M. I. Arshad, S. Ikram, U. Rehman and S. Hussain, Tailoring the thermoelectric properties of sol-gel grown CZTS/ITO thin films by controlling the secondary phases, *Phys. B Condens. Matter*, 2019, **558**, 86–90.

24   T. J. Seebeck, Ueber die magnetische Polarisation der Metalle und Erze durch Temperatur-Differenz, *Ann. Phys.*, 1826, **82**, 133–160.

25   M. R. Burton, T. Liu, J. McGettrick, S. Mehraban, J. Baker, A. Pockett, T. Watson, O. Fenwick and M. J. Carnie, Thin Film Tin Selenide (SnSe) Thermoelectric Generators Exhibiting Ultralow Thermal Conductivity, *Adv. Mater.*, 2018, **30**, 1801357.

26   A. A. Talin, A. Centrone, A. C. Ford, M. E. Foster, V. Stavila, P. Haney, R. A. Kinney, V. Szalai, F. El Gabaly, H. P. Yoon, F. Léonard and M. D. Allendorf, Tunable electrical conductivity in metal-organic framework thin-film devices, *Science (80-.).*, 2014, **343**, 66–69.

27   M. Ilami, R. J. Ahmed, D. Edwards, E. Thompson, S. Zeinolabedinzadeh and H. Marvi, Magnetically Actuated Tunable Soft Electronics, *ACS Omega*, 2019, **4**, 21242–21250.

28   T. Heine, Transition metal chalcogenides: Ultrathin inorganic materials with tunable electronic properties, *Acc. Chem. Res.*, 2015, **48**, 65–72.

29   Y. Liu, E. Mu, Z. Wu, Z. Che, F. Sun, X. Fu, F. Wang, X. Wang and Z. Hu, Ultrathin MEMS thermoelectric generator with Bi2Te3/(Pt, Au) multilayers and Sb2Te3 legs, *Nano Converg.*, , DOI:10.1186/s40580-020-0218-x.

30   G. J. Snyder, J. R. Lim, C. K. Huang and J. P. Fleurial, Thermoelectric microdevice fabricated by a

MEMS-like electrochemical process, *Nat. Mater.*, 2003, **2**, 528–531.

31   Z. Zhang and Y. Ma, DC-25 GHz and low-loss MEMS thermoelectric power sensors with floating thermal slug and reliable back cavity based on GaAs MMIC technology, *Micromachines*, , DOI:10.3390/mi9040154.

32   C. Gould and N. Shammas, in *Micro Electronic and Mechanical Systems*, 2009, p. 572.

33   U. Syafiq, N. Ataollahi, R. Di Maggio and P. Scardi, Solution-Based Synthesis and Characterization of Cu2ZnSnS4 (CZTS) Thin Films, *Molecules*, 2019, **24**, 3454.

34   N. Ataollahi, C. Malerba, R. Ciancio, R. Edla, P. Scardi, E. Cappelletto and R. Di Maggio, Control of composition and grain growth in Cu2ZnSnS4 thin films from nanoparticle inks, *Thin Solid Films*, 2019, **674**, 12–21.

35   N. Ataollahi, F. Bazerla, C. Malerba, A. Chiappini, M. Ferrari, R. Di Maggio and P. Scardi, Synthesis and post-annealing of Cu2ZnSnS4 absorber layers based on Oleylamine/1-dodecanethiol, *Materials (Basel).*, 2019, **12**, 3320.

36   P. Scardi and M. Leoni, Whole powder pattern modelling, *Acta Crystallogr. Sect. A Found. Crystallogr.*, 2002, **58**, 190–200.

37   P. Scardi, C. L. Azanza Ricardo, C. Perez-Demydenko and A. A. Coelho, Whole powder pattern modelling macros for TOPAS, *J. Appl. Crystallogr.*, 2018, **51**, 1752–1765.

38   M. Leoni, T. Confente and P. Scardi, PM2K: A flexible program implementing Whole Powder Pattern Modelling, *Zeitschrift fur Krist. Suppl.*, 2006, **1**, 249–254.

39   V. Linseis, F. Völklein, H. Reith, K. Nielsch and P. Woias, Advanced platform for the in-plane ZT measurement of thin films, *Rev. Sci. Instrum.*, , DOI:10.1063/1.5005807.

40   T. Liu, X. Zhao, J. Li, Z. Liu, F. Liscio, S. Milita, B. C. Schroeder and O. Fenwick, Enhanced control of self-doping in halide perovskites for improved thermoelectric performance, *Nat. Commun.*, 2019, **10**, 1–9.

41   T. Liu, S. Y. Yue, S. Ratnasingham, T. Degousée, P. Varsini, J. Briscoe, M. A. McLachlan, M. Hu and O. Fenwick, Unusual Thermal Boundary Resistance in Halide Perovskites: A Way to Tune Ultralow Thermal Conductivity for Thermoelectrics, *ACS Appl. Mater. Interfaces*, 2019, **11**, 47507–47515.

42   A. Lafond, L. Choubrac, C. Guillot-Deudon, P. Deniard and S. Jobic, Crystal structures of photovoltaic chalcogenides, an intricate puzzle to solve: The cases of CIGSe and CZTS materials, *Zeitschrift fur Anorg. und Allg. Chemie*, 2012, **638**, 2571–2577.

43   R. E. Dinnebier, A. Leineweber and J. S. O. Evans, *Preface*, 2018.

44   J. J. S. Scragg, L. Choubrac, A. Lafond, T. Ericson and C. Platzer-Björkman, A low-temperature order-disorder transition in Cu2ZnSnS4 thin films, *Appl. Phys. Lett.*, 2014, **104**, 041911.

45   J. J. S. Scragg, J. K. Larsen, M. Kumar, C. Persson, J. Sendler and S. Siebentritt, Cu–Zn disorder and band gap fluctuations in Cu2ZnSn(S,Se)4: Theoretical and experimental investigations, *Phys. Satus Solidi B*, 2016, **253**, 247–254.

46   A. Khare, B. Himmetoglu, M. Johnson, D. J. Norris, M. Cococcioni and E. S. Aydil, Calculation of the lattice dynamics and Raman spectra of copper zinc tin chalcogenides and comparison to experiments, *J. Appl. Phys.*, , DOI:10.1063/1.4704191.

47   K. Rudisch, Y. Ren, C. Platzer-Bjorkman and J. Scragg, Order-disorder transition in B-type Cu2ZnSnS4 and limitations of ordering through thermal treatments, *Appl. Phys. Lett.*, 2016, 231902.

48   Y. Pei, X. Shi, A. Lalonde, H. Wang, L. Chen and G. J. Snyder, Convergence of electronic bands for high

performance bulk thermoelectrics, *Nature*, 2011, **473**, 66–69.

49   W. G. Zeier, H. Zhu, Z. M. Gibbs, G. Ceder, W. Tremel and G. J. Snyder, Band convergence in the non-cubic chalcopyrite compounds Cu2MGeSe4, *J. Mater. Chem. C*, 2014, **2**, 10189–10194.

50   M. Hegedus, M. Achimovičová, H. Hui, G. Guélou, P. Lemoine, I. Fourati, J. Juraszek, B. Malaman, P. Baláž and E. Guilmeau, Promoted crystallisation and cationic ordering in thermoelectric Cu26V2Sn6S32 colusite by eccentric vibratory ball milling, *Dalt. Trans.*, , DOI:10.1039/d0dt03368e.

51   P. Baláž, M. Achimovičová, M. Baláž, K. Chen, O. Dobrozhan, E. Guilmeau, J. Hejtmánek, K. Knížek, L. Kubíčková, P. Levinský, V. Puchý, M. J. Reece, P. Varga and R. Zhang, Thermoelectric Cu–S-Based Materials Synthesized via a Scalable Mechanochemical Process, *ACS Sustain. Chem. Eng.*, , DOI:10.1021/acssuschemeng.0c05555.

52   S. Englund, V. Paneta, D. Primetzhofer, Y. Ren, O. Donzel-Gargand, J. K. Larsen, J. Scragg and C. Platzer Björkman, Characterization of TiN back contact interlayers with varied thickness for Cu2ZnSn(S,Se)4 thin film solar cells, *Thin Solid Films*, 2017, **639**, 91–97.

53   N. Saini, J. K. Larsen, K. V. Sopiha, J. Keller, N. Ross and C. Platzer-Björkman, Germanium Incorporation in Cu2ZnSnS4 and Formation of a Sn–Ge Gradient, *Phys. Status Solidi Appl. Mater. Sci.*, 2019, **216**, 1–12.

54   N. M. Martin, C. Platzer-Björkman, K. Simonov, H. Rensmo and T. Törndahl, Passivation of CdS/Cu2ZnSnS4 Interface from Surface Treatments of Kesterite-Based Thin-Film Solar Cells, *Phys. Status Solidi Basic Res.*, , DOI:10.1002/pssb.202000308.

55   J. K. Larsen, F. Larsson, T. Törndahl, N. Saini, L. Riekehr, Y. Ren, A. Biswal, D. Hauschild, L. Weinhardt, C. Heske and C. Platzer-Björkman, Cadmium Free Cu2ZnSnS4 Solar Cells with 9.7% Efficiency, *Adv. Energy Mater.*, 2019, **9**, 1–8.

56   E. Isotta, B. Mukherjee, C. Fanciulli and N. M. Pugno, Order parameter from the Seebeck coefficient in thermoelectric kesterite Cu2ZnSnS4, *Proc. TMS*.